Determination of Size and Refractive Index of a Single Water Droplet by Using a Light Source with Short Coherence Length (LED)

Walter Schäfer[1], Cameron Tropea[1,3], Wolfgang Elsäßer[2,3]

1: Institute of Fluid Mechanics and Aerodynamics, Technische Universität Darmstadt, Germany,
w.schaefer@sla.tu-darmstadt.de and ctropea@sla.tu-darmstadt.de
2: Institute of Applied Physics, Technische Universität Darmstadt, Germany,
wolfgang.elsaesser@physik.tu-darmstadt.de
3: Center of Smart Interface, Technische Universität Darmstadt, Germany

Abstract The use of short coherence length light sources for optical particle characterization offers a number of interesting features, whose potential have not yet been fully explored or exploited. For one, such light sources can be considerably less expensive than lasers, with particular reference to high-intensity and highly durable LEDs (light emitting diodes). Furthermore, as with femtosecond light sources, the short coherence length suppresses interference between various scattering orders in the far field, leading to a more monotonic intensity dependence as a function of particle size. The lack of polarization can contribute in the same manner to a reduction of interference phenomena. This can be especially attractive if intensity or intensity ratio measures are to be used in estimating particle characteristics. What is not clear is which measurement principles can best exploit these features.
The present work investigates the use of glare point imaging for estimating size and refractive index of spherical, transparent particles/droplets. Two measures are used to determine these two quantities, the separation between the reflective and 2nd order refractive glare points, and the intensity ratio between the two. A velocity measurement is not considered, but could be easily implemented using a time-of-flight measurement through two illuminating sheets or by multiple imaging and a particle tracking approach.

1. Introduction

Methods of optical particle characterization, in cases where they can be applied, are clearly preferred over alternative techniques due to their non-intrusiveness and convenience in terms of *in-situ* application. Therefore, efforts to widen the range of applicability of various methods have not abated, fueled often by the availability of new, improved, more powerful or less expensive hardware components. In this particular study, the possibilities for particle characterization afforded by high-intensity light emitting diodes (LED) are explored. The question arises, which measurement principle can best exploit such light sources? An overview of currently used principles and their respective measurement capabilities is given in Table 1. From these options, the present work concentrates on using direct imaging, through the imaging of glare points, and an intensity ratio method, to estimate particle size and refractive index. The analysis is carried out assuming spherical, transparent particles, in this particular case liquid droplets are used. For most applications a velocity measurement is also required, in particular if concentrations or fluxes are to be estimated. This aspect will not be considered in the present study, but an extension of the present work using a time-of-flight measurement, or through the use of multiple exposures (particle tracking) could be envisioned.

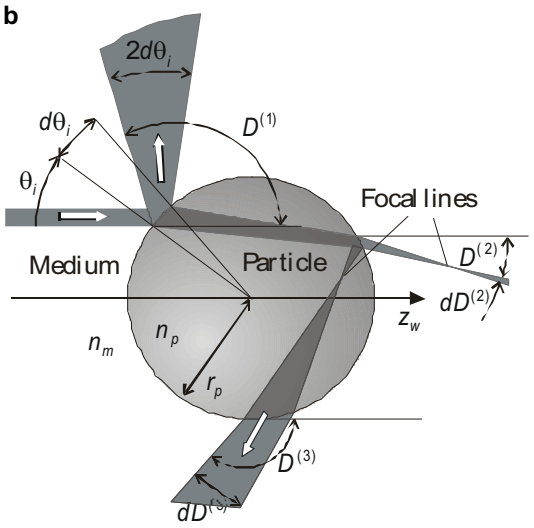

Figure 1: Focussing of a finite width ‚pencil of light' on a spherical particle [1]

Table 1: Overview of measurement principles for optical particle characterization

Measurement Principle	**Measured Quantity**	**Measurement Technique**
Direct Imaging	velocity, size, shape	PIV/PTV, shadowgraphy, glare point separation
Intensity, Intensity ratio	size, temperature, species	extinction/absorption, modulation depth, MIE/LIF ratio, two-/three-band LIF,
Interferometry	velocity, size, refractive index /temperature	laser Doppler, phase Doppler, ILIDS/IPI, diffraction, rainbow refractometry, holography
Time-Shift	size, velocity	time-of-flight, pulse displacement, time-shift technique
Pulse Delay	size, temperature	femtosecond laser methods
Raman-Scattering	temperature, species concentration	Raman spectroscopy

Glare point refers to an intensity maximum seen when a particle illuminated by a wide beam is viewed from a certain direction and imaged [1]. Figure 1, taken from [2] illustrates the origin of three glare points on a spherical particle with a relative refractive index larger than unity $m>1$ (m - relative refractive index $m=n_p/n_0$; n_p - refractive index of particle; n_0 - refractive index of surrounding medium). For a given scattering angle, i.e. the angle of the detector, several glare points may be observable at different intensities, the intensity being a function of the scattering order and scattering angle. Such information is available for a plane homogeneous illuminating wave by using the Lorenz-Mie Theory (LMT) [3, 4]. Debye [5] and later van der Pol and Bremmer [6] interpreted the scattered light in terms of different scattering orders (p=0 reflection, p=1 first-order refraction, etc.). This is also intuitively compatible to a geometric optics (GO) description, valid for larger particles (Glantsching and Chen [7], van de Hulst [8]).

Imaging of glare points for measurement of particle size distributions is by no means new, as described already by van de Hulst and Wang [1]. If the image is out of focus, the ILIDS (interferometric laser imaging for droplet sizing) is invoked, as first introduced by Glover et al. [9] and later developed by numerous further researchers [10, 11, 12, 13]. The present work concentrates however, on the in-focus imaging of the glare points, as discussed in detail in Hess [10] and more recently by Hess and L'Esperance [14]. The separation of glare points can be directly related to the particle size, knowing the order of the glare points being observed and the relative refractive index. In [14] the technique was extended to smaller particles – and small separations - by utilizing the polarizing properties of the scattered light to distinguish between two, very closely spaced glare points of order p=0 (reflective) and p=1 (first-order refraction).

In the following work, we have restricted ourselves to larger particles and furthermore, an effort was made to achieve an optical arrangement in which the detector was placed more in a backscatter direction, in an effort to conduct the measurement with a single optical access.

If both the size and the relative refractive index are unknown, then the glare point separation alone will not be sufficient to characterize the particle. In this case further information is required. Intensity is often considered as an option, since intensity does relate to particle size. The intensity of glare points of course also exhibits a size dependence, this is illustrated in figure 1, in which the shown illuminating 'pencil of light' is either more or less focused at various glare points. Of course the actual 'pencil of light' observed will be defined by the aperture of the receiver. The basic drawback of intensity based methods is however, that intensity is not strictly a monotonic function of size, at least for Lorenz-Mie scattering. The intensity fluctuations arise due to the interference of various scattering orders at a given detection (scattering) angle. Intensity based methods attempting

to circumvent this difficulty have been proposed in the past [15, 16]; however these have generally be discouraged, since intensity is also a function of many other factors, many of which are uncontrollable in a real experiment, e.g. obscuration in dense sprays, dirty optical windows, etc.). More promising are intensity ratio based methods, in which, at least the external factors can be cancelled out. Mie/LIF (Laser-induced Fluorescence) belong to this category, in which the intensity of the fluorescent field is approximately monotonic with size [17,18]. The strategy in the current work is to recover a monotonic intensity dependence on size by eliminating interference between different scattering orders, which should be possible once the coherence length of light decreases below the path-length difference of different scattering orders at a given scattering angle.

2. Light Source and Experimental Setup

Light emitting diodes were used as a light source in this study. A blue LED was used (LXK2-PR14-R00) from the Luxeon K2® product line of Phillips Lumileds Lighting Co. The blue LED has a center wavelength of 465 nm at an optical power of 500 mW using 1000mA current. The FWHM is about 20 nm, as shown in the measured spectrum shown in Figure 2. The coherence length is given approximately by the relation

$$L_C \approx \frac{\lambda^2}{\Delta\lambda} \tag{1}$$

yielding a value of 10µm. This coherence length was confirmed separately with a measurement using a Michelson interferometer. The use of short coherence length lasers has been previous reported in the literature [19]. In that particular application, an incoherent semiconductor laser (ISL) with a coherence length of 120 µm was employed. The main perceived advantage of using an LED over an ISL is the lower cost. In [20] the incoherent feature of a femtosecond light source suppressed the ripple structure of the first rainbow significantly, allowing a better estimation of particle size from the Airy theory.

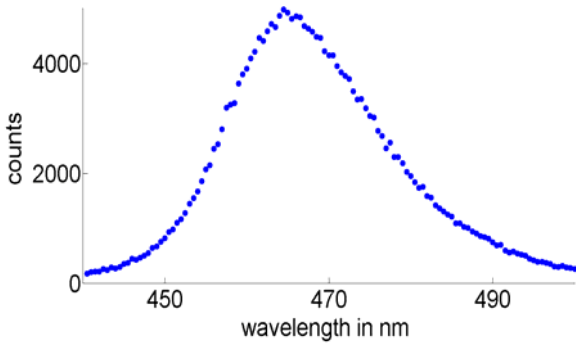

Figure 2: Wavelength spectrum of royal blue LED (Phillips LXK2-PR14-R00)

The optical arrangement to record the scattered light is illustrated schematically in Figure 3. A liquid droplet was held in the path of a blue or red LED by means of an acoustic levitator. The droplet was slightly deformed to an oblate shape due to gravity, but this was inconsequential to the present study, since measurements were performed on the equator of the droplet. However the acoustic levitator is not able to stably hold small droplets; hence the lower limit of droplet size was about 70µm. The initial diameter of injected droplets into the levitator was between 300 and 500µm. Liquid droplets (distilled water or water/acetone mixtures) were used and these evaporated down to 70µm in typically 1 minute, allowing the scattered light to be observed by a CCD camera at 0.5s intervals throughout the evaporation phase.

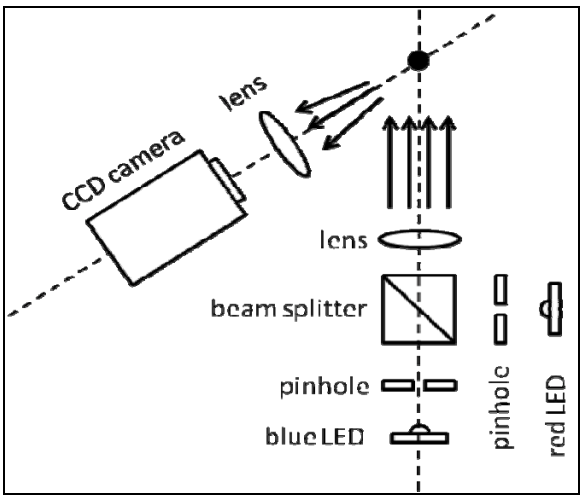

Figure 3: Schematic illustration of the experimental setup

3. Results

3.1 Far-field scattering

To begin, we examine the far-field scattering for two different particle diameters, 50 and 200µm. These results have been computed according to the Lorenz-Mie Theory and illustrated using the Debye series decomposition for the first five scattering orders, see Figure 4. Note that these results are computed using the LED wavelength spectrum shown in figure 2. The light was not polarized so that the intensity is given as the square root of the sum of the intensities from parallel and perpendicularly polarized light. From these results we see that in the near-backscatter direction, the two dominant scattering orders are reflection (+diffraction) (p=0) and second-order refraction (p=2). At a scattering angle of about 120 deg, the two dominating orders are reflection (p=0) and third-order refraction (p=3).

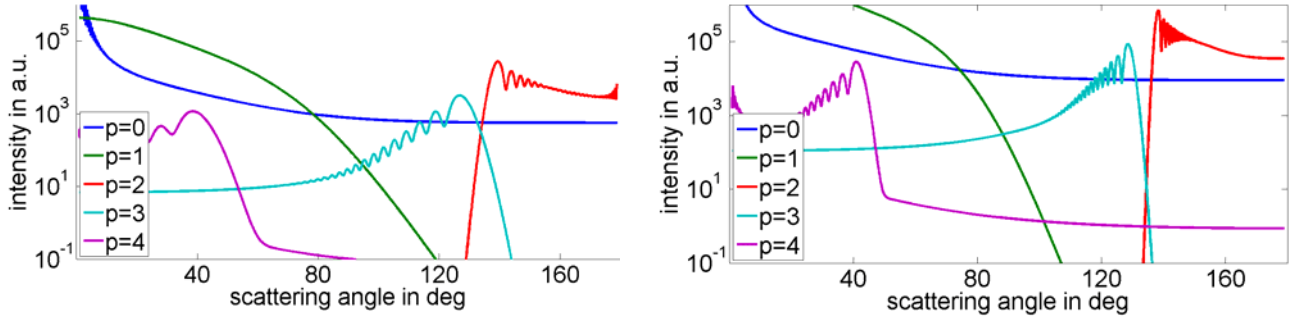

Figure 4: Far-field scattering intensity computed using LMT for a water droplet in air (m=1.33) Left d_p=50µm, Right d_p=200µm

The oscillations of p=2 and p=3 in the scattering range 120-150 deg correspond to the first and second rainbows. These oscillations arise through interference of two different modes of the same scattering order. For an extremely short coherence length, shorter that the path length difference between the two modes, these oscillations should disappear. In the present case of 10µm coherence length and particles of 50 and 200µm, the interference is still observable. To illustrate this even clearer, further LMT computations were performed in the scattering angle range of the first rainbow (135 – 180 deg). The scattered intensity for a single wavelength (λ=465nm) is compared to the intensity using the wavelength spectrum shown in figure 2. This comparison is given in Figure 5 for 50µm and 200 µm particles (m=1.33). From this comparison it becomes clear that the path-length difference at the main rainbow lobe is far less than 10µm, here the interference between the two modes of second-order refraction (p=2) is the same for both light sources. However at higher scattering angles, especially for the larger droplet, the path-length difference has increased beyond the 10µm and interference with the LED is significantly reduced.

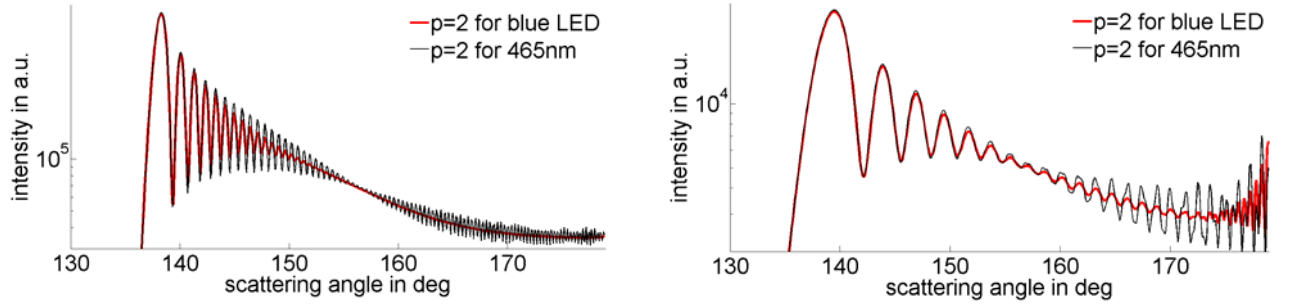

Figure 5: Far-field scattering intensity computed using LMT for a water droplet in air (m=1.33) Left d_p=200µm, Right d_p=50µm. Computations at a single wavelength (λ=465nm) are compared to those using a wavelength spectrum of the blue LED.

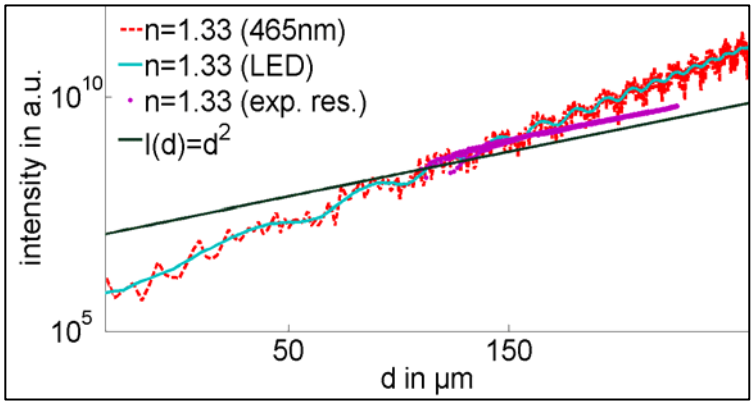

Figure 6: Scattered light intensity for a scattering angle of 117°.

The expected and measured scattering properties of the water droplet as a function of droplet size are summarized in Figure 6 for various light sources and for a scattering angle of 117°. Note that at this scattering angle, the dominant scattering orders are reflection and third-order refraction. The first curve in the diagram corresponds to a computed curve using the Lorenz-Mie theory. As expected, this curve exhibits a strong non-monotonic behavior, corresponding to the second rainbow. The second curve is also a computed intensity curve, this time for the blue LED, taking into account the wavelength spectrum of the broadband light source, as illustrated in Fig. 2. This superposition of various wavelengths already smoothes the lobe structure of the intensity curve considerably. The next curve is the measured intensity as the droplet evaporates from about 200µm to 70 µm and exhibits a very monotonic dependence on size. This result is highly repeatable. Experimentally the interference is still further reduced over the computational result. As a reference, a d^2-line is superimposed on the diagram, since in this range of size, a d^2 dependence is to be expected. Note that the size range 50m to 200µm corresponds to a Mie parameter $(\pi d/\lambda)$ of 320 to 1300, well into a range normally suitable for treatment using geometric optics. This suggests that the fundamental difficulty associated with an intensity measurement, i.e. the non-monotonic behavior with size, is overcome with the short coherence length LED, even in the vicinity of rainbows. However a calibration would still be necessary if intensity alone is used – note that the curves in Fig. 5 are given in arbitrary units and this for a constant and known relative refractive index.

3.2 Glare points

The information to be gained from the in-focus imaged glare points is their position relative to the particle boundaries, or the separation between two or more glare points. Therefore, first the dependencies of the glare point positions will be examined, in particular the dependence on scattering angle and relative refractive index. The position of the glare point will be given as a normalized quantity, i.e. made dimensionless with the particle diameter, since the position should not be size dependent, at least to a first approximation.

The angular position of the normalized glare point of reflection (p=0) is not dependent on refractive index. The incident angle $\theta_i^{p=0}$ for the reflection [2] is given by

$$\sin(\theta_i^{p=0}) = \cos\left(\frac{\theta_s}{2}\right) \qquad (2)$$

where θ_s is the scattering angle. Because the position of this normalized glare point is independent of relative refractive index, it can be used in principle as a reference point for determining the refractive index.

The position of the normalized glare points of second-order refraction depends on refractive index for a constant scattering angle [1]. This incident angle $\theta_i^{p=2}$ can be determined by solving the equation

$$m\sin\left(\frac{\theta_i^{p=2}}{2} + \frac{\pi}{4} - \frac{\theta_S}{4}\right) = \sin\left(\theta_i^{p=2}\right) \qquad (3)$$

numerically, where m is the relative refractive index. This results in the following relation for the normalized separation between the two glare points, reflection and second-order refraction:

$$\left|\frac{\vec{r}^{(p=0)} - \vec{r}^{(p=2)}}{d}\right|(\theta = const) \propto m = \frac{n_p}{n_0} \tag{4}$$

showing that the distance between glares points at a constant scattering angle decreases with refractive index. This relation allows the relative refractive index to be determined experimentally, in principle.

The numerical and experimental results pertaining to these relations are presented in figure 7, where also the position of the third-order refractive glare point is shown. The experimental and numerical results for reflection (p=0) show a good agreement. For second-order refraction (p=2) some minor deviations between theory and experiment are observed. There is some uncertainty associated with determining the position of the glare point experimentally. Even an imprecise droplet size determination will affect this result, since the size is used as a non-dimensionalizing quantity. These uncertainties are currently being characterized in more detail.

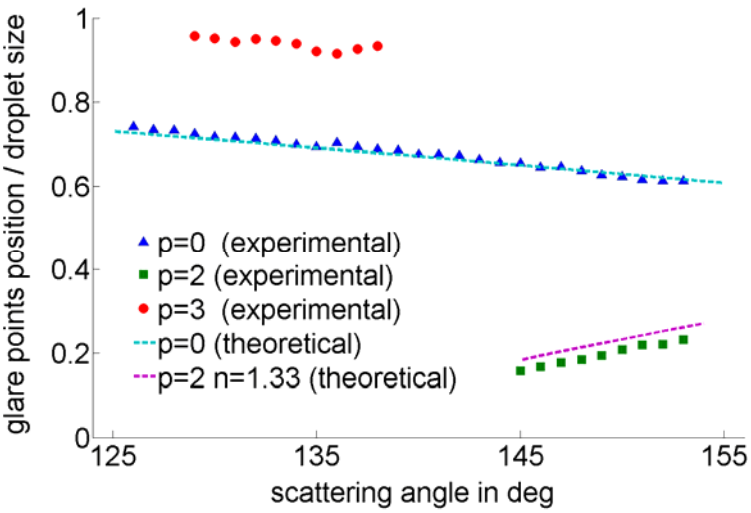

Figure 7: Normalized glare point position. Symbols are experimental results, solid lines are empirical fits, and dashed lines are numerical calculated.

In the next measurements the relative refractive index has been varied by examining either water droplets or acetone/water mixtures. The normalized glare point position for second-order refraction (p=2) is shown in Fig. 8 as a function of scattering angle and for different relative refractive indexes. The position of the reflection glare points remain the same as in figure 7. The relative refractive index of the acetone/water mixture is larger than for pure water and the experimental results exhibit this trend. Nevertheless, the quantitative agreement between experiment and theory is not excellent and further work is required to localize the main sources of discrepancy

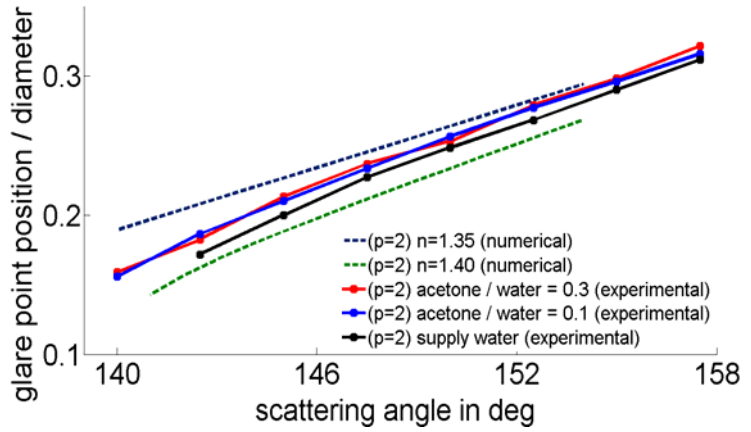

Figure 8: Numerical and experimental results of second-order refraction for angle range from 140 to 158 deg. Dashed lines are numerical results and lines are experimental results.

3.3 Intensity ratio

The intensity ratio between the glare point of reflection and the glare point of the second-order refraction can be used for estimating the particle size. In order to find the intensity ratio, it is necessary to first determine some analytical description of the intensities of the reflection and of the second-order refraction as a function of the droplet size d and the refractive index n_p (assuming

n_0 is 1) for a constant angle θ. In general these intensities can be written in the functional form

$$I^{(p=0,2)}(n,d,\theta=const)=C_{p=0,2}(n)f^{(p=0,2)}(d) \quad (5)$$

with the corresponding limiting conditions

$$I^{(p=0,2)}(d=0,n,\theta=const)=0$$
$$I^{(p=0,2)}(d,n=1,\theta=const)=0 \quad (6)$$

The numerical calculation for an LED spectrum of the reflection and second-order refraction for a scattering angle of 160 deg and different refractive indexes as a function of droplet size is shown in figure 9. The numerical calculated curves from this figure have been fitted using

$$I^{(p=0,2)}(d,n,\theta=160°)=C_{p=0,2}(n)d^2 \quad (7)$$

where $C_{(p=0,2)}(n)$ is a function of the refractive index. The value of these coefficients as a function of refractive index are shown in figure 10. These coefficients can also be fitted using polynomial expressions:

$$C_{p=0}(n)=1.115n^2-1.80n+0.65 \quad (8)$$

$$C_{p=2}(n)=10^5(-0.64n^5+4.1n^4-11n^3+14n^2-8.9n+2.3) \quad (9)$$

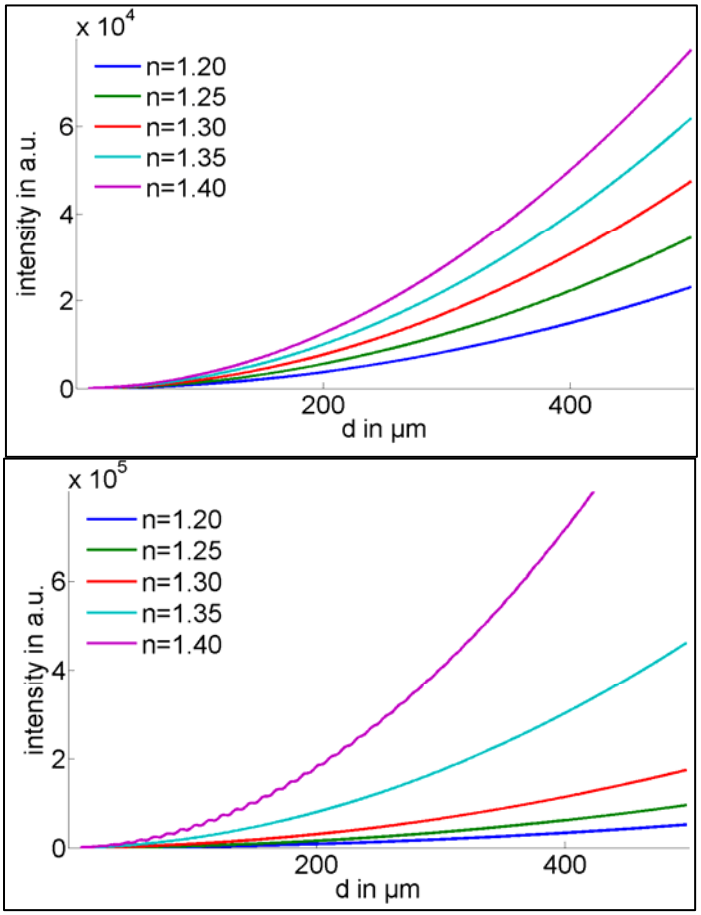

Figure 9: The intensity of the reflection (above) and of the second-order refraction (lower) as a function of the droplet size for the different refractive index at a constant angle of 160 deg. Calculated for the spectrum of the blue LED. Ordinate scale same for both graphs.

where $n\in[1.2:1.4]$ and $d\in[10:500]\mu m$.

After the dependency of the considered intensities on droplet size and refractive index are known, the intensity ratio can be written as

$$\frac{I^{(p=2)}(d,n,\theta=160°)}{I^{(p=0)}(d,n,\theta=160°)}=\frac{C_{p=2}(n)d^2}{C_{p=0}(n)d^2}=C_{20}(n) \quad (10)$$

where $C_{20}(n)$ can be found numerically or can be calibrated with an experiment.

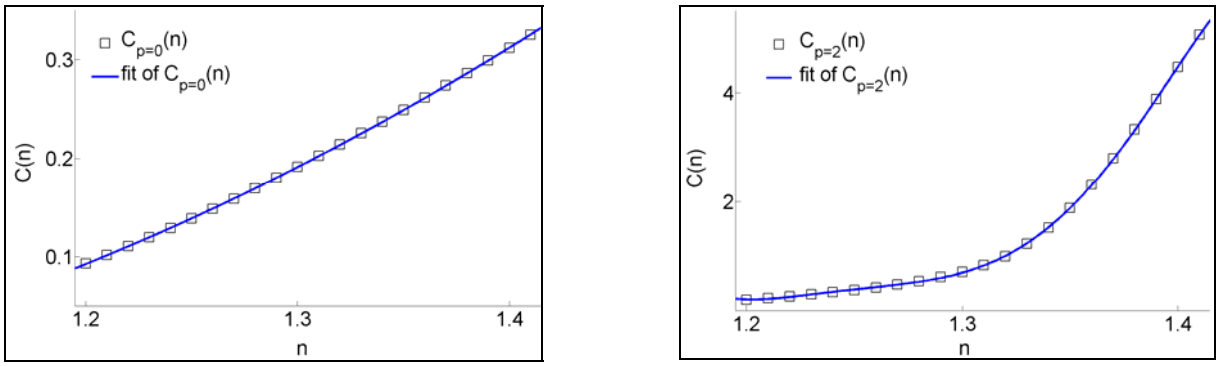

Figure 10: The coefficients from the fitted curves of figure 9. Left plot is for reflective glare point, right plot is for second-order refractive glare point.

4. Summary and Conclusions

The present study explores the possibility of employing high lumens per package LED light sources for optical particle characterization, with a goal of lower component costs in practical measurement systems. In particular the short coherence length feature has been examined in terms of consequences on the scattered light intensity as a function of particle size. For certain backscatter directions, at which reflective and second-order refractive scattering orders are roughly equal in intensity, a smoothening of the intensity-size relation could be demonstrated theoretically and experimentally. This opens the way to employing an intensity ratio approach to estimate particle size. Furthermore, the glare point separation is available as a measured quantity, dependent on relative refractive index and scattering angle. The strategy would be to determine the relative refractive index from glare point separation and then the size from the intensity ratio.

Nevertheless, much is still to be investigated before viable measurement systems can be designed. The influence of polarization has not yet be discussed; the present assumption is that the LEDs are randomly polarized, thus also inhibiting any interference of different scattering orders. A second topic concerns the measurement uncertainties involved, in particular in determining the glare point position and intensity. These uncertainties will surely increase dramatically for very small particles, while the non-monotonic behavior of the intensity-size curve will tend to increase. So a practical lower measurable size limit will arise, as yet not estimated. Finally, the technique here must be integrated into a velocity measurement scheme, to provide individual particle velocities necessary for estimating fluxes. Finally, one can remark that this technique offers the possibility of extension to a planar measurement method.

Acknowledgements

The authors acknowledge the financial support of the Deutsche Forschungsgemeinschaft through the Research Training Group GRK 1114.

References

[1] van de Hulst HC, Wang RT. (1991) Glare points. *Appl. Opt*. **30**:4755-4763.

[2] Albrecht HE, Borys M, Damaschke N, Tropea C. (2003) **Laser Doppler and Phase Doppler Measurement Techniques**. Springer-Verlag, Berlin, Heidelberg.

[3] Lorenz L. (1890) Lysbevaegeisen i og uden for en hal plane lysbôlger belyst kluge. *Vidensk Selk Skr.* **6**:1-62.

[4] Mie G. (1908) Beiträge zur Optik trüber Medien, speziell kolloidaler Metallösungen, *Annalen der Physik.*, **330**: 377-445.

[5] Debye (Debije) P. (1908) Das elektromagnetische Feld um einen Zylinder und die Theorie des Regenbogens. *Physikalische Zeitschift* **9**:775-778.

[6] van der Pol B, Bremmer H. (1937) Diffraction of electromagnetic waves from a point source. *Phio. Mag.* **24**:141-190 and 825-864

[7] Glantsching WJ, Chen SH. (1981) Light scattering from water droplets in the geometrical optics approximation. *Appl. Opt*. **20**:2499-2509.

[8] van de Hulst HC. (1981) **Light Scattering by Small Particles**. Dover Publications, New York.

[9] Glover AR, Skippon SM, Boyle RD. (1995) Interferometric laser imaging for droplet sizing: a method for droplet-size measurement in sparse spray systems. *Appl. Opt.* **34**:8409-8421.

[10] Hess CF. (1998) Planar particle image analyzer. *9th Int. Symp. on Appl. of Laser Techn. to Fluid Mech., Lisbon, Portugal*. Paper 18.1.

[11] Maeda M, Kawaguchi T, Hishida K. (2000) Novel interferometric measurement of size and velocity distributions of spherical particles in fluid flows. *Meas. Sci. Technol.* **11**:L13-L18.

[12] Kawaguchi T, Akasaka Y, Maeda M. (2002) Size measurement of droplets and bubbles by advanced interferometric laser imaging technique. *Meas. Sci. Technol.* **13**:308-316.

[13] Damaschke N, Nobach H, Nonn TI, Semidetnov N, Tropea C. (2005) Multi-dimensional particle sizing techniques. *Exp. in Fluids*. **39**:336-350.

[14] Hess CF, L'Esperance D. (2009) Droplet imaging velocimeter and sizer: a two-dimensional technique to measure droplet size. *Exp. in Fluids*, **47**:171-182.

[15] Farmer WM. (1972) Measurement of particle size, number density, and velocity using a laser interferometer. *Appl. Opt*. **11**:2603-2612.

[16] Bachalo WD. (1980) A method for measuring the size and velocity of spheres by dual beam light scatter interferometry. *Appl. Opt*. **19**:363-370.
[17] Domann R, Hardalupas Y. (2001) Spatial distribution of fluorescence intensity within large droplets and ist dependence on dye concentration. *Appl. Opt*. **40**:3586-3597.
[18] Frackowiak B, Tropea C. (2010) Numerical analysis of the diameter influence on droplet fluorescence. *Appl. Opt*. **49:**2363-2370.
[19] Peil M, Fischer I, Elsäßer W, Bakic S, Damaschke N, Tropea C, Stry S, Sacher J. (2006) Rainbow refractometry with a tailored incoherent semiconductor laser source, Appl. Phys. Lett. **89**:091106.
[20] Bakic S, Xu F, Damaschke N, Tropea C. (2009) Feasibility of extending rainbow refractometry to small particles using femtosecond laser pulses. *Part. Part. Syst. Charact.* **26:**34-40.